Research Article Vol. 59, No. 5 / 10 February 2020 / Applied Optics A213

applied optics

Designing with very thin optical films

RONALD R. WILLEY,[1,*] AUDRIUS VALAVIČIUS,[2] AND FRED T. GOLDSTEIN[3]

[1]Willey Optical, Consultants, 13039 Cedar Street, Charlevoix, Michigan 49720, USA
[2]Optical Coating Laboratory, Center for Physical Sciences and Technology, Savanorių Ave. 231, Vilnius LT-02300, Lithuania
[3]FTG Software Associates, P.O. Box 579, Princeton, New Jersey 08542, USA
*Corresponding author: ron@willeyoptical.com

Received 20 November 2019; revised 16 January 2020; accepted 16 January 2020; posted 17 January 2020 (Doc. ID 383929); published 6 February 2020

There is increasing interest in the design of films with thicknesses on the order of 10 nm and less for a variety of applications, such as nanoparticles, plasmonics, quantum dots, solar reflectors, black mirrors, etc. The indices of refraction (*n* and *k*) for the effective media of such coatings depend on the materials with which such "layers" interface and the specific process parameters used to produce those films. The structures may typically be nucleating island structures and may also be continuous films. A key factor is that the *n* and *k* values vary in thickness until some thickness is obtained, usually >20 nm. Heretofore, to the best of our knowledge, films have not taken into account thickness index variations during the design process. Software has now been developed where the index at a given thickness is computed at each iteration of the design optimization process. This allows more realistic design results utilizing the full representation of the behavior of the layers in question; the resulting coatings, when produced, are in better agreement with the designs. Including *n* and *k* versus wavelength and thickness in the design process is here referred to as *double dispersion*.

https://doi.org/10.1364/AO.383929

1. INTRODUCTION

Optical thin film design typically uses the simplifying assumption that real films are homogeneous in terms of their thickness, although this is known to be only an approximation. Layers thinner than 10 nm in optical thin film designs are commonly avoided, probably due to the uncertainty of the index of such layers as a function of thickness. The first stages of optical thin film formation might be likened to rain falling on a dry surface. In some cases, it might look like dry pavement where the drops wet the surface and spread. In other cases, it might be more like a rain droplet on the polished hood of an automobile. These nucleation differences are apparently caused by the energy and surface tension relationships of the surfaces and the depositing material. The net result can be small separated islands to which new atoms are drawn when they have some residual mobility on the surfaces until the islands have grown large enough to touch each other or coalesce into a continuous surface coating. Another result can be more like surface wetting, where the coating eventually coalesces and covers the surface with a continuous film.

Foteinopolou *et al.* recently introduced a feature issue in *Optical Materials Express* [1], "Beyond Thin Films: Photonics with Ultrathin and Atomically Thin Materials," which emphasizes the broad current interest in these very thin films in both pre-coalesced and continuous forms. Various of these papers [2–9] deal with films on the order of 10 nm thick, and some are dealing with films whose index variation with thickness must be considered in the coating design processes such as is discussed here.

Consider a film monitored by a quartz crystal microbalance (QCM). After a few nanometers have registered, the actual peaks of the islands are usually several times (to an order of magnitude) higher than the QCM reading, because the material droplets are stacked up, and not spread evenly over the surface. With many materials, the coalescence occurs at about 10–20 nm as read on a QCM. If the conditions promote wetting as reported by Formica *et al.* [10] using a very thin precoat of copper (Cu) or other materials, the coalescence might occur at only a few nm of QCM reading.

The net effect of the described behavior of the nucleating atoms in a new layer is that the indices of refraction are quite different as a function of the thickness for most layer materials until thicknesses of several tens of nm are reached. These very thin layers are used in modern applications such as solar control coatings, black mirrors, metamaterials, and plasmonic structures. To realistically model such systems, it is necessary to know how the *n* and *k* of these layers vary with thickness, and to incorporate that knowledge into the thin film design process. A solar control coating might have three silver (Ag) layers on the order of 10 nm thick, separated by much thicker dielectric layers, plus *another very thin layer* for additional absorptance as described by

Medwick *et al.* [11]. Similarly, a black mirror might have two or three layers of chromium (Cr) that are less than 10 nm thick.

Stenzel and Macleod [12] have provided a very extensive tutorial on the technology related to the present paper. They pointed out that the accepted approach was to acknowledge that the index of very thin films did vary with thickness and therefore needed to be characterized at each thickness of interest. The designer should pick a specific thickness that had been characterized and hold that thickness constant, while varying the other layers of the design. They state that "The thickness of a metal island film must not be varied during a design procedure. A metal island film with a given thickness and given effective optical constants has to be tackled as a fixed building block which can be introduced into an interference stack, but should not be modified during the synthesis and refinement." They also later state: "A limitation that is missing from normal coating design is the strict constraint on the thickness of the composites and this is something that we must accept." This present report deals with relieving this constraint and the expansion of the capability of the design software to allow the metal island or other variable index film to vary in thickness *during* the design process in a realistic way.

2. EXPERIMENTAL DETAILS

Fused silica (FS) substrates 25.4 mm in diameter and 1 mm in thickness were used. Substrate roughness was <0.7 nm. All substrates were cleaned in a four-stage ultrasonic cleaning system UCS40 (Optimal Technologies) before the deposition process; more details are given in Ref. [13].

The sample structure was FS substrate/alumina 7 nm/silver X nm/alumina 7 nm. Dielectric layers were deposited using the atomic layer deposition (ALD) technique. The bottom dielectric layers were used to evaluate the same initial growth conditions and morphology for silver nanoparticles. The top layer stabilizes and protects the silver nanoparticles from environment influence.

The silver islands were deposited using a thermal evaporation system VERA1100. The base pressure of $<1 \times 10^{-5}$ mbar was reached by the rotary and cryogenic pumps. Silver deposition processes were implemented using thermal resistivity heating in molybdenum crucible filled with silver pellets. The silver purity used for the experiment was of >99.99%. The deposition rate was fixed at 0.5 Å/s. The deposition temperature for silver was 20–23°C. The given nominal silver thickness value corresponds to mass-thickness equivalents. The deposited material nominal thickness was controlled by a QCM system.

Alumina layers were deposited in a cross-flow type ALD reactor Savannah S200 manufactured by VEECO. Nitrogen (purity 99.999%) was used as a carrier and as a purging gas with a constant 20 SCCM flow. Commercial trimethylaluminium (TMA) and deionized water were used as reactants for the alumina layers. The pulse for TMA and water was for 0.02 s at a time. The duration of purge cycle of TMA and water excess and reaction products was 6 s. The reactor temperature during the deposition process was 150°C. To obtain the desired layer thickness of 7 nm, 70 cycles were deposited.

The samples optical properties of reflection (R) and transmittance (T) were measured for averaged polarization at the incidence (reflected) angle of 8° in the $300 < \lambda < 1300$ nm wavelength range using a Photon RT (Essent Optics) spectrophotometer.

ALD was used due to its property to form a uniform dense layer that repeats the surface morphology. Also the ALD technology allows the deposition of one atomic layer thickness per cycle. The film was exposed to the ambient two times: first after forming the alumina back layer, and second after depositing the silver layer. In both cases, the sample was in ambient for less than 10 min. The copper (if used) and silver layers were deposited without breaking a vacuum in the same run. The ALD process should affect the silver layer by a small rearrangement because the reactor temperature was at 150°C (the silver formation process was at 20°C). The heating procedure took 30 min.

3. DATA ACQUISITION

As will be shown, the n and k versus thickness can be a strong function of the materials and processes used on both sides of the variable thickness layers. The characterization layers need to be first deposited on a substrate or layer of the preceding material, then the variable index layer, and then a capping layer of the following material. All of these depositions are to be done by the processes to be used in the intended application. It is necessary to perform enough test runs at different thicknesses to cover the gamut of layer thicknesses expected to be used in actual designs. If there is any significant question as to the near-linearity of the n and k between the sampled thicknesses, more thickness samples may need to be taken. The typical measurements from which to best derive the n and k are the near-normal incidence transmittance (%T), reflectance (%R) of the coating from the coated side (%Rfwd), and reflectance from the reverse side (%Rrev). The n and k could also be acquired by ellipsometric methods [8] and other choices of %R, %T, angle, and thickness.

The procedure used to determine the n and k indices versus wavelength was to measure the near-normal percent of %R and %T versus wavelength for each of the different thickness samples prepared as above. These data were then entered in the FilmStar [14] software as targets for optimization by varying n and k, as seen, for example, in the solid curves of Fig. 1. In these cases, the target %R and %T at 1300 nm were used, and

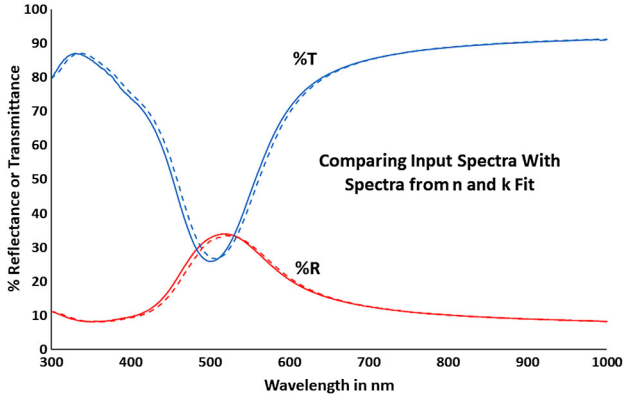

Fig. 1. %R and %T versus wavelength for 2 nm thicknesses of Ag deposited on FS in air.

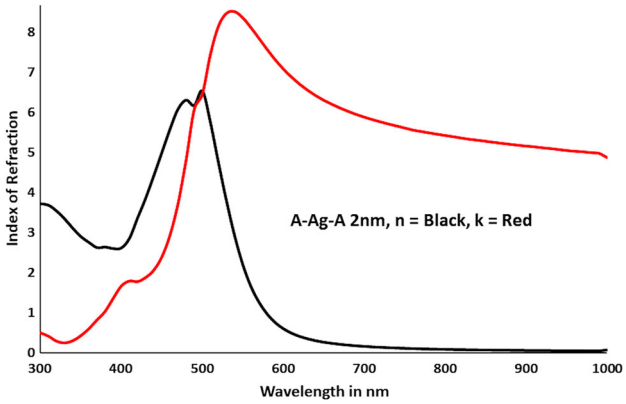

Fig. 2. Derived n (black) and k (red) versus wavelength for 2 nm thicknesses of Ag deposited on FS in air.

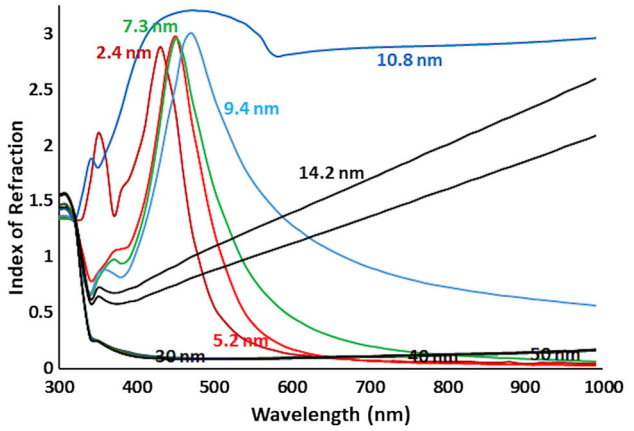

Fig. 3. Index (n) versus wavelength for various thicknesses of Ag deposited on FS in air.

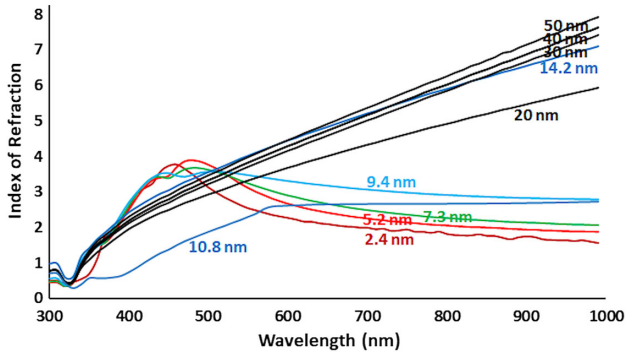

Fig. 4. Index (k) versus wavelength for various thicknesses of Ag deposited on FS in air.

the effective thickness was found by optimization. The software then keeps this effective thickness fixed for that sample and uses the %T and %R values for each single wavelength sequentially in order from the longest to the shortest, and finds the n and k values which produce that %R and %T. No index function such as Cauchy or Sellmeier is used in this fitting process. Tables of these indices versus wavelength are stored as would be any other material indices and identified by a name that includes their nominal QCM thickness. Figure 2 shows the n and k thus determined. The derived n and k values were then used to calculate the %R and %T, which are then plotted as dashed lines in Fig. 1 for comparison with the original values from which the n and k were derived to determine the quality of the fit.

Various modeling schemes such as polynomials and Bruggeman theory, as discussed in Hummel and Guenther [15], were considered to fit n and k versus wavelength and thickness to the measurements. However, it was decided that real n and k curves of a variety of materials are too varied in shape for these models to be practical. Therefore, the chosen approach is to use the n and k determined from spectral measurements at the deposited thicknesses and interpolate the n and k for in between thicknesses. Normally three to six test thicknesses have proved to be adequate, although nine are currently possible. For each different material combination and process, a user-programable dispersion formula utilizes the multiple individual index tables deduced from fixed thickness measurements.

The materials interfacing with both sides of the thin metal layers are commonly dielectrics such as silica, alumina, etc. We have noticed no effects of the thickness of these dielectric layers on the effective n and k properties of the thin metal layers, only the optical phases in the design relationships. The software deals with these spacer/dielectric layers in the usual manner as layers whose index does not vary with thickness.

4. DESIGNING WITH VARIABLE INDEX LAYERS

In the optical thin film design process of FilmStar [14], when a variable index versus thickness layer is encountered, the layer's identifying code indicates that n and k vary with thickness and wavelength. When the evaluation process reaches that layer, it generates a temporary n and k versus wavelength value to be used for that layer at that thickness for that *one time*. It does this by determining between which two thicknesses the n and k have been evaluated by experiment, and then simply linearly interpolating between those two. The optimization process otherwise proceeds normally. The optimization algorithms that can be chosen are damped least squares, Levenberg–Marquart, and simplex. The computing times are increased somewhat from that of non-variable index layers by the interpolation process; however, the effect is negligible on modern computers. If the thickness of a layer is less than that of those evaluated to develop the table, n and k are assumed to be the same as that of the thinnest layer actually evaluated; and similarly, if the layer is thicker than the thickest evaluated, it is assumed to have the same n and k as that of the thickest layer evaluated.

Figures 3 and 4 illustrate how radically the n and k can vary with thickness in silver films deposited on FS. At a 2.4–9.4 nm thickness, island formation is apparent, and plasmonic behavior seems to come into play. In the region beyond the 9.4 nm thickness, there seems to be some coalescence, whereas 20 nm shows a move toward a continuous film, and 30 nm seems to behave more like bulk silver. Although this bare silver in air might never be used in practice, it is a strong example of the variability of the n and k with thickness.

Figures 5–8 plot a different view of the n and k versus *thickness* and wavelength for two different designs and material interfaces. Figures 5 and 7 are for silver deposited on FS in air, and

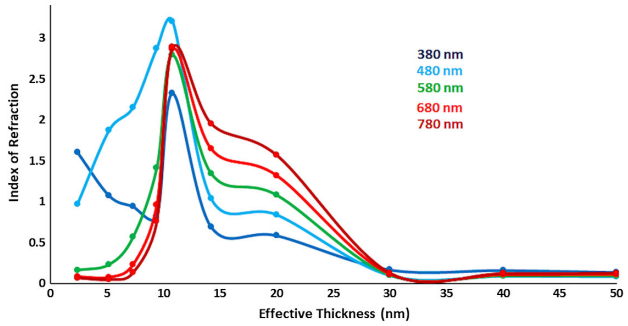

Fig. 5. Index (n) versus thickness for various wavelengths of Ag deposited on FS in air.

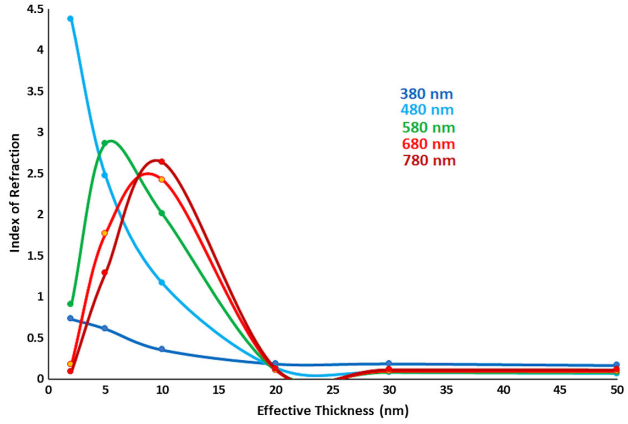

Fig. 6. Index (n) versus thickness for various wavelengths of Ag deposited on alumina and capped with alumina.

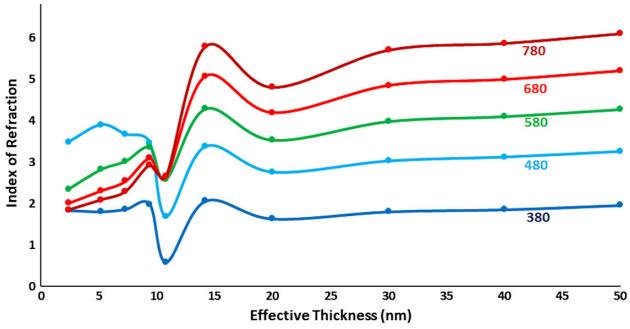

Fig. 7. Index (k) versus thickness for various wavelengths of Ag deposited on FS in air.

Figs. 6 and 8 for FS substrates coated with 7 nm of alumina (via ALD), then the silver layer, and then are capped with 7 nm of alumina (via ALD). These figures illustrate the influence of the materials that interface with the silver. Small errors in the fitting process and the characteristics of Excel plotting sometimes give the appearance of negative n and k values. These negative values are not considered to be physically real.

Figures 9 and 10 show the use of the interpolation software to compare various coatings and processes on a common basis at the same thickness of 5 nm. They also show how strong the variations are between Ag and the interface materials and processes

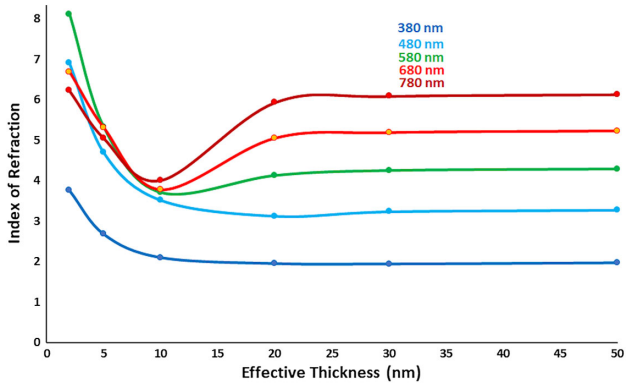

Fig. 8. Index (k) versus thickness for various wavelengths of Ag deposited on alumina and capped with alumina.

for samples that are all of the same thickness. The solid-line and dotted-line Ag processes were done by our colleagues Andrius Valavičius *et al.* [16].

The dashed-line process in Figs. 9 and 10 using Zn_2SnO_4 is from Medwick *et al.* [11], and the indium tin oxide (ITO) process is from Hernandez-Mainet *et al.* [17]. The interpolation process was used for Figs. 9 and 10 to be able to compare all processes at the same thickness (5 nm). These n and k plots point to the fact that the Medwick process at 5 nm was mostly coalesced and approaching the bulk characteristics, while the FS/Ag in air was still in an island phase. The other two materials/processes appear to be in intermediate transition phases.

5. EXPERIMENTAL DEMONSTRATION OF TECHNIQUE

A simple test case was designed to demonstrate the application of this technique. The design goal was to find the thickness of the silver layer that would provide the highest reflection at the peak in the 500–550 nm region. Figure 11 shows the design that was 3.3 nm thick and provided 35.5% reflection. This figure shows that a 5 nm film has a lower peak %R, and 1 nm also has a lower peak %R. Thicknesses that are ±10% of the nominal 3.3 nm (3.0 and 3.63) are also plotted. The inset in the upper right of Fig. 11 shows the design details as represented in the software. Because the ALD process is conformal and coats all exposed sides of a part, the back of the substrates get two coats of 7 nm for a total of 14 nm thickness of Al_2O_3 by the time all of the layers have been deposited.

These five designs were actually produced by the same processes used to produce the index files for the thin silver layer between 7 nm layers of alumina on 1 mm FS substrates. These experimental results are shown in Fig. 12. The results are in general agreement with the designs and verify that the maximum %R at the 500–550 nm region from the design process is in fact achieved at a silver thickness of approximately 3.3 nm. Differences between Figs. 11 and 12 illustrate the difficulties in obtaining the exact reproducibility on this nano-scale and with process variability. It would appear that the application of ALD in the future to these kinds of films could improve uniformity, thickness control, and reproducibility.

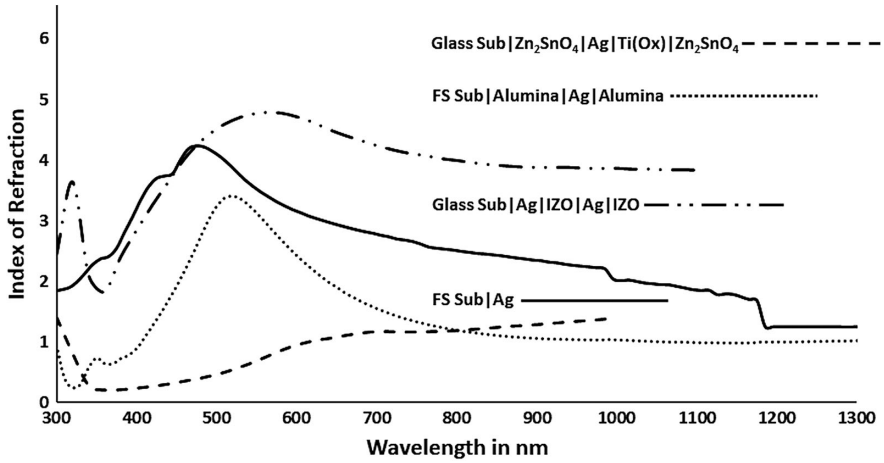

Fig. 9. Index (n) versus wavelength for various processes and interfaces of a 5-nm-thick Ag layer.

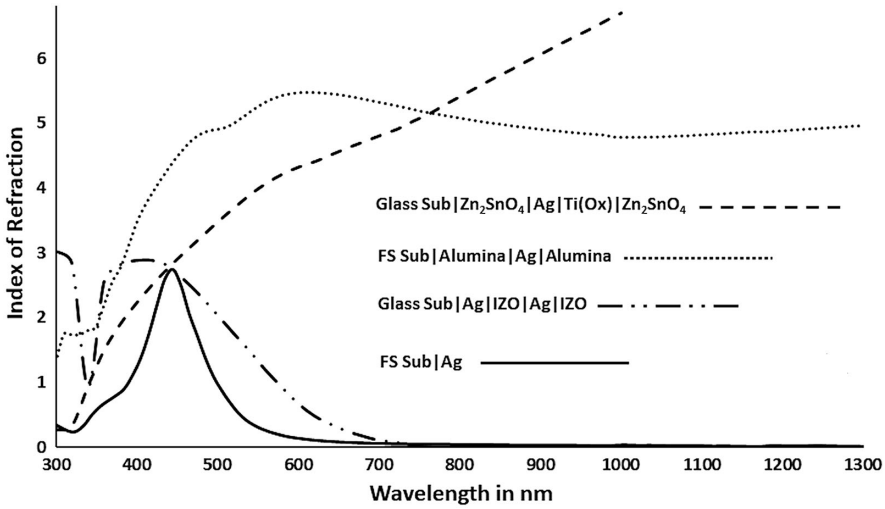

Fig. 10. Index (k) versus wavelength for various processes and interfaces of a 5-nm-thick Ag layer.

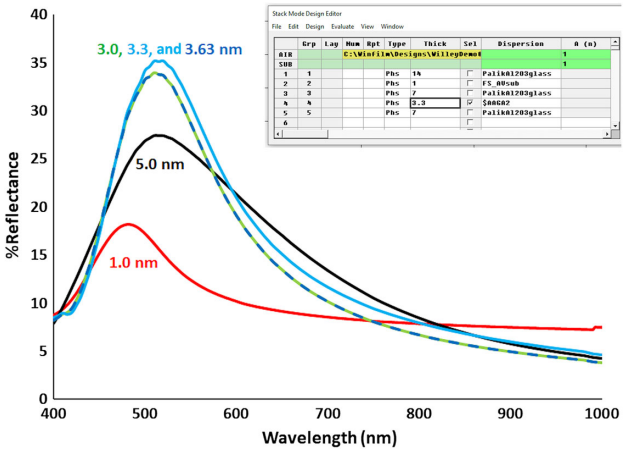

Fig. 11. Design of 3.3-nm-thick silver to maximize %R at 500 nm. Reflectance of thicknesses surrounding 3.3 nm.

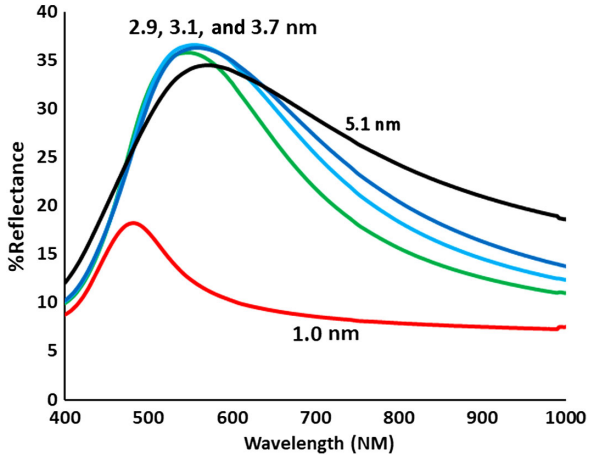

Fig. 12. Spectral results of deposited films per the designs of Fig. 11 and the effective thicknesses of those films.

The effective indices used in these interpolation files were derived by fitting the indices from real sample spectra taken from samples of nominal effective thicknesses of 2, 5, 10, 20, 30, and 50 nm. A 1 nm silver sample was not available at the time. The thickness numbers given in Fig. 12 are those provided by the computer fitting of n, k, and *effective* thickness, and

not by any real physical measure. One decimal place might be representative of the real error bounds.

6. CONCLUSION

It is clear that some materials and processes show a strong variation in indices with thickness for very thin layers, up through the point of coalescence, that is, before bulk properties are established. This can also be true for some materials and processes after coalescence. Realization of this design and fabrication process has been demonstrated by a simple example. Very thin layers are used now more frequently than ever before for solar energy control, black mirrors, metamaterial applications, plasmonic applications, etc., where the design tools described herein are needed to more properly apply the real variation of indices with thickness.

REFERENCES

1. S. Foteinopolou, N. C. Panoiu, V. M. Shalaev, and G. S. Subramania, "Photonics with ultrathin and atomically thin materials," Opt. Mater. Express **9**, 2427–2436 (2019).
2. A. Milewska, A. S. Ingason, O. E. Sigurjonsson, and K. Leosson, "Herding cats: managing gold atoms on common transparent dielectrics," Opt. Mater. Express **9**, 112–119 (2019).
3. C.-H. Liu, J. Zheng, Y. Chen, T. Fryett, and A. Majumdar, "Van der Waals materials integrated nanophotonic devices," Opt. Mater. Express **9**, 384–399 (2019).
4. A. S. Baburin, A. M. Merzlikin, A. V. Baryshev, I. A. Ryzhikov, Y. V. Panfilov, and I. A. Rodionov, "Silver-based plasmonics: golden material platform and application challenges," Opt. Mater. Express **9**, 611–642 (2019).
5. Y. Wang, J. Xiao, S. Yang, Y. Wang, and X. Zhang, "Second harmonic generation spectroscopy on two-dimensional materials," Opt. Mater. Express **9**, 1136–1149 (2019).
6. H. Taghinejad, A. A. Eftekhar, and A. Adibi, "Lateral and vertical heterostructures in two-dimensional transition-metal dichalcogenides," Opt. Mater. Express **9**, 1590–1607 (2019).
7. A. S. Roberts, M. Chirumamilla, D. Wang, L. An, K. Pedersen, N. A. Mortensen, and S. I. Bozhevolnyi, "Ultra-thin titanium nitride films for refractory spectral selectivity [Invited]," Opt. Mater. Express **8**, 3717–3728 (2018).
8. R. Secondo, D. Fomra, N. Izyumskaya, V. Avrutin, J. N. Hilfiker, A. Martin, Ü. Özgür, and N. Kinsey, "Reliable modeling of ultrathin alternative plasmonic materials using spectroscopic ellipsometry [Invited]," Opt. Mater. Express **9**, 760–770 (2019).
9. H. Knopf, N. Lundt, T. Bucher, S. Höfling, S. Tongay, T. Taniguchi, K. Watanabe, I. Staude, U. Schulz, C. Schneider, and F. Eilenberger, "Integration of atomically thin layers of transition metal dichalcogenides into high-Q, monolithic Bragg-cavities: an experimental platform for the enhancement of the optical interaction in 2D-materials," Opt. Mater. Express **9**, 598–610 (2019).
10. N. Formica, D. S. Ghosh, A. Carrilero, T. L. Chen, R. E. Simpson, and V. Pruneri, "Ultrastable and atomically smooth ultrathin silver films grown on a copper seed layer," ACS Appl. Mater. Interface **5**, 3048−3053 (2013).
11. P. A. Medwick, A. V. Wagner, P. J. Fisher, and A. D. Polcyn, "Nanoplasmonic ('sub-critical') silver as optically absorptive layers in solar-control glasses," in *60th Annual Technical Conference Proceedings*, Providence, Rhode Island (Society of Vacuum Coaters, 2017).
12. O. Stenzel and A. Macleod, "Metal-dielectric composite optical coatings: underlying physics, main models, characterization, design and application aspects," Adv. Opt. Technol. **1**, 463–481 (2012).
13. K. Juškevičius, R. Buzelis, G. Abromavičius, R. Samuilovas, S. Abbas, A. Belosludtsev, R. Drazdys, and S. Kičas, "Argon plasma etching of fused silica substrates for manufacturing high laser damage resistance optical interference coatings," Opt. Mater. Express **7**, 3598 (2017).
14. FilmStar, "FTG software associates," FTGSoftware.com.
15. R. E. Hummel and K. H. Guenther, *Handbook of Optical Properties* (CRC Press, 1995), Vol. **I**, p. 312.
16. A. Valavicius, P. Jurksaits, S. Kicas, and A. Belosludtsev, "Optimization of thermal evaporation for continuous silver films and their application for non-polarizing optical components," Proc. SPIE **10691**, 106911Y (2018).
17. L. C. Hernandez-Mainet, M. A. Aguilar, M. C. Tamargo, and C. Falcony, "Design and engineering of IZO/Ag/glass solar filters for low-emissivity window performance," Opt. Eng. **56**, 105103 (2017).